Aitken mode particles as CCN in aerosol- and updraft-sensitive regimes of cloud droplet formation

Mira L. Pöhlker[1], Minghui Zhang[2], Ramon Campos Braga[1], Ovid O. Krüger[1], Ulrich Pöschl[1], and Barbara Ervens[2]

[1]Multiphase Chemistry Department, Max Planck Institute for Chemistry, 55128 Mainz, Germany
[2]Université Clermont Auvergne, CNRS, SIGMA Clermont, Institut de Chimie de Clermont-Ferrand, 63000 Clermont-Ferrand, France

Correspondence: Mira Pöhlker (m.pohlker@mpic.de), Barbara Ervens (barbara.ervens@uca.fr)

Abstract. The high variability of aerosol particle concentrations, sizes and chemical composition makes their description challenging in atmospheric models. Aerosol-cloud interaction studies are usually focused on the activation of accumulation mode particles as cloud condensation nuclei (CCN). However, under specific conditions also Aitken mode particles can contribute to the number concentration of cloud droplets (N_d), leading to large uncertainties in predicted cloud properties on a global scale. We perform sensitivity studies with an adiabatic cloud parcel model to constrain conditions, under which Aitken mode particles contribute to N_d. The simulations cover wide ranges of aerosol properties, such as total particle number concentration, hygroscopicity (κ) and mode diameters for accumulation and Aitken mode particles. Building upon the previously suggested concept of updraft (w)- and aerosol-limited regimes of cloud droplet formation, we show that activation of Aitken mode particles does not occur in w-limited regimes of accumulation mode particles. The transitional range between the regimes is broadened when Aitken mode particles contribute to N_d, as aerosol-limitation requires much higher w than for aerosol size distributions with accumulation mode particles only. In the transitional regime, N_d is similarly dependent on w and κ. Therefore, we analyze the sensitivity of N_d to κ, $\xi(\kappa)$, as a function of w to identify the value combinations, above which Aitken mode particles can affect N_d. As $\xi(\kappa)$ shows a minimum when the smallest activated particle size is in the range of the 'Hoppel minimum' (0.06 µm $\leq D_{min} \leq$ 0.08 µm), the corresponding (w,κ) pairs can be considered a threshold level, above which Aitken mode particles have significant impact on N_d. This threshold is largely determined by the number concentration of accumulation mode particles and by the Aitken mode diameter. Our analysis of these thresholds results in a simple parametric framework and criterion to identify aerosol and updraft conditions, under which Aitken mode particles are expected to affect aerosol-cloud interactions. Our results confirm that Aitken mode particles likely do not contribute to N_d in polluted air masses (urban, biomass burning) at moderate updraft velocities ($w \leq 3$ m s^{-1}), but may be important in deep convective clouds. Under clean conditions, such as in the Amazon, the Arctic, and remote ocean regions, hygroscopic Aitken mode particles can act as CCN at updrafts of $w <$ 1 m s^{-1}.

1 Introduction

The representation of aerosol-cloud interactions in atmospheric models is challenging due to the high variability of aerosol particle loading, properties and processes on small temporal and spatial scales. Aerosol-cloud interactions include both the effects of aerosol particles on clouds by acting as cloud condensation nuclei (CCN) and the modification of aerosol due to chemical and physical cloud processing.

The interaction of aerosol particles with water vapor is described by the Köhler theory (Köhler, 1936). It combines the curvature (Kelvin) effect that describes the enhancement of the water vapor pressure above a curved particle surface and the solute (Raoult) effect that accounts for water uptake by hygroscopic particle mass which is often parameterized by the hygroscopicity parameter κ (Petters and Kreidenweis, 2007). The maximum of the Köhler curve represents the critical supersaturation (S_{crit}), above which a particle of a given composition and dry size (critical diameter, D_{crit}) is activated and efficiently grows to a cloud droplet.

Clouds are dynamic systems where the supersaturation is continuously altered due to increasing water vapor concentration in cooling air parcels and other processes and water vapor condensation onto particles. As the supply of water vapor and the growth time scales in clouds are limited, particles and droplets may not reach their equilibrium sizes. Thus, conclusions based on equilibrium conditions as implied by Köhler theory often represent overestimates of the effect of aerosol properties on clouds, e.g., Ervens et al. (2005).

The relative importance of aerosol parameters (e.g., chemical composition (κ), dry particle diameter (D), shape of aerosol size distribution (ASD), particle number concentration (N_a)) and updraft velocity (w) on cloud properties were explored in previous sensitivity studies. Feingold (2003) showed that N_a has the largest influence on the effective radius of a cloud droplet size population, followed by the geometric mean mode diameters and standard deviations of aerosol size distributions (ASDs) (D_g and σ_g). A similar ranking was discussed by Pardo et al. (2019) who showed that conclusions regarding the relative importance of the aerosol properties and w hold true for both the effective droplet radius and number concentration (N_d) with lower sensitivity of the effective radius than that of N_d. Other sensitivity studies also identified w and N_a, followed by κ and other chemical composition effects, as the most important parameters determining N_d (Ervens et al., 2005; McFiggans et al., 2006; Anttila and Kerminen, 2007; Reutter et al., 2009; Ward et al., 2010) or the supersaturation in clouds (Hammer et al., 2015). Similar relative importances of N_a, and w on the shape of the cloud droplet size distribution (CDSD) were shown (Cecchini et al., 2017).

CCN can be modified in clouds by mass addition due chemical reactions in cloud droplets and by collision-coalescence processes (e.g., Ervens, 2015). These processes are suggested to lead to a size separation of cloud-processed and interstitial particles, resulting in a gap between the Aitken and accumulation modes ('Hoppel minimum') (Hoppel et al., 1986; Cantrell et al., 1999; Feingold and Kreidenweis, 2000). It is traditionally assumed that only accumulation mode particles (D > $\sim$ 0.07 µm) undergo cloud-processing leading possibly to a broadening of this mode.

Model and observational studies challenge this assumption, as ambient conditions were identified under which supersaturation in clouds is sufficiently high to form cloud droplets on Aitken mode particles. For example, at a continental remote

background site in France, Aitken mode particles with $D \geq \sim$0.025 µm were shown to contribute the major fraction to N_d due to the absence of a significant accumulation mode (Gérémy et al., 2000). About 30% of all Aitken mode particles were observed to form cloud droplets at a background site in Finland at very low N_a ($\sim$150 cm^{-3}) (Komppula et al., 2005). Similarly low aerosol loading was encountered above the tropical ocean, where $\leq$ 40% of Aitken mode particles were predicted to act as CCN (Roelofs et al., 2006). Also in Arctic clouds, high contributions of Aitken mode particles to N_d were predicted (Korhonen et al., 2008; Jung et al., 2018; Bulatovic et al., 2020). In marine stratocumuli off the Californian coast, CCN and droplet closure could be only achieved when contributions of Aitken mode particles to N_d were taken into account in clouds with $w \geq 0.6$ m s^{-1} (Schulze et al., 2020). In deep convective clouds above the Amazon ($w \leq 12$ m s^{-1}), it was predicted that the formation of cloud droplets on Aitken mode particles (D $\geq$ 0.02 µm) might even impact the thermodynamic cloud structure by amplifying the convective invigoration and affecting precipitation rates (Fan et al., 2018).

Based on an intercomparison of 16 global models, it was concluded that Aitken mode particles do not significantly contribute to CCN in clouds with maximum supersaturations S_{max} = 0.2% (Fanourgakis et al., 2019). Based on another global model study, Lee et al. (2013) compared the influence of 28 parameters characterizing aerosol emissions, processes and size distributions on the CCN number concentration at S = 0.3%. They identified the width of the Aitken mode as the second most impo‘rtant parameter, after the dry deposition of accumulation mode particles. Chang et al. (2017) found that on a global scale, the fraction of Aitken mode particles to total CCN is negligible at S = 0.2 % while it can be significant at S = 0.4% above the continental northern hemisphere. In their later global model study, cloud supersaturation in each grid cell was calculated based on the mean vertical velocity, and N_d was derived as the number of particles whose S_{crit} that was approximated and compared for three cloud activation schemes (Chang et al., 2021). While the schemes mostly agreed in the N_d prediction from accumulation mode particles, large discrepancies predictions were found in the contribution of Aitken mode particles to N_d.

These prior studies provide strong evidence that Aitken mode particles can cause large uncertainties in predicted aerosol-cloud interactions under conditions of low N_a, small fractions of accumulation mode particles to total N_a and/or high w. In the current study, we perform simulations with an adiabatic parcel model to systematically explore the parameter ranges of aerosol properties (N_a, $N_{a,Ait}/N_{a,acc}$, κ, $D_{g,Ait}$, $D_{g,acc}$) and of w to identify aerosol and cloud conditions, under which Aitken mode particles contribute to N_d. (All parameters are defined Table A1 in the Appendix.) Our analysis results in a framework that can be used to assess under which aerosol and cloud conditions detailed information on Aitken mode particles is needed to describe their potential role in aerosol-cloud interactions.

2 Adiabatic parcel model

2.1 Model description

We use an adiabatic parcel model to examine droplet formation on a population of aerosol particles (Feingold and Heymsfield, 1992; Ervens et al., 2005). The evolution of particle and droplet sizes is described on a moving size grid. The calculation of the equilibrium saturation (s_{eq}) is based on Köhler theory, including the hygroscopicity parameter κ (Petters and Kreidenweis,

2007; Rose et al., 2008).

$$s_{eq} = \left(1 + \kappa \frac{V_s}{V_w}\right)^{-1} \exp\left(\frac{4\sigma_{sol} M_w}{RT\rho_w D_{wet}}\right) \tag{E.1}$$

whereas D_{wet} is the wet particle diameter, σ_{sol} the surface tension of the wet particle (72 mN m^{-1}), ρ_s the density of the dry particle, ρ_w the density of pure water, M_w the molecular weight of water, *R* the constant for ideal gases and *T* the absolute temperature.

We note that we do not consider additional composition effects (such as surface tension suppression) as κ represents the effective hygroscopicity as derived from experimental data. The model includes the standard thermodynamic equations for particle and droplet growth and the derivatives to time of temperature, saturation and pressure (Pruppacher and Klett, 2003). These differential equations are iteratively solved within each model time step. The times steps are function of *w* and chosen such that they cover a vertical change of the air parcel of 0.1 m . The change in the saturation is calculated as

$$\frac{ds}{dt} = \underbrace{\Psi_1 w}_{updraft\ term} - \underbrace{\Psi_2 2\pi \frac{\rho_w}{\rho_s} G \int D_{wet} N_a(D)(s - s_{eq}) dD_{wet}}_{condensation\ term} \tag{E.2}$$

where Ψ_1 and Ψ_2 are functions of temperature and saturation (*s*). The updraft term describes the increase of *s* due to cooling of a rising air parcel in an adiabatic environment; the condensation term accounts for the condensation of water vapor on aerosol particles and droplets. Particle and droplet growth is driven by the gradient between *s* and the particle-specific s_{eq}:

$$\frac{dD_{wet}}{dt} \propto \frac{(s - s_{eq})}{D_{wet}} \tag{E.3}$$

2.2 Model simulations

2.2.1 Initialization

The model is initialized below cloud at RH = 98%, T = 290 K, and p = 829 mbar. The initial ASDs consist of 545 particle size classes in a diameter range of 0.0028 µm < D < 1.4 µm, in lognormal distributions with geometric mean mode diameters $D_{g,Ait}$ = 0.037 µm and $D_{g,acc}$ = 0.145 µm with standard deviations of σ_g = 0.5 (corresponding to 1.4 in commonly used Heisenberg fits). Note, that different versions of lognormal fit functions are used in the literature (Pöhlker et al., 2021); a standard lognormal fit function was applied here (Pöhlker et al., 2018).

In sensitivity tests, $D_{g,Ait}$ and $D_{g,acc}$ are shifted to 0.05, 0.06 and 0.07 µm and to 0.13 and 0.17 µm, respectively (Section 3.3.2). We define 15 model ASDs that differ (i) in the relative contributions of Aitken and accumulation mode particles ($N_{a,Ait}$, $N_{a,acc}$) to total N_a (columns I - V in Figure 1), and (ii) in the total number concentration N_a (rows a - c in Figure 1). ASDs I and V are monomodal with an accumulation or Aitken mode only; ASDs II, III and IV are bimodal with $N_{a,Ait}$ corresponding to 50% (ASD II), 100% (ASD III) and 150% (ASD IV) of $N_{a,acc}$. We distinguish the two modes by the diameter of the Hoppel

minimum (∼0.07 μm). While strictly both modes have 'tails' beyond the Hoppel minimum (Aitken mode particles being larger and accumulation mode particles being smaller than the Hoppel minimum), we do not consider this in our model. This simplification seems justified since the mode classification in measured ASDs are usually ascribed based on particle size and not based composition which may differ because of different sources of particles in the two modes. The particle hygroscopicity is assumed to be equal in both modes; 27 values are used in the simulations to cover a range of $0.02 \leq \kappa \leq 1$. Additional tests are performed for fixed κ values in the accumulation mode (κ_{acc} = 0.1 and 0.5; Section 3.3.1). 30 values for the updraft velocities are applied (0.1 m s^{-1} $\leq w \leq$ 3 m s^{-1}), resulting in 810 simulations (27 $\kappa\times$ 30 w) for each of the 15 ASDs.

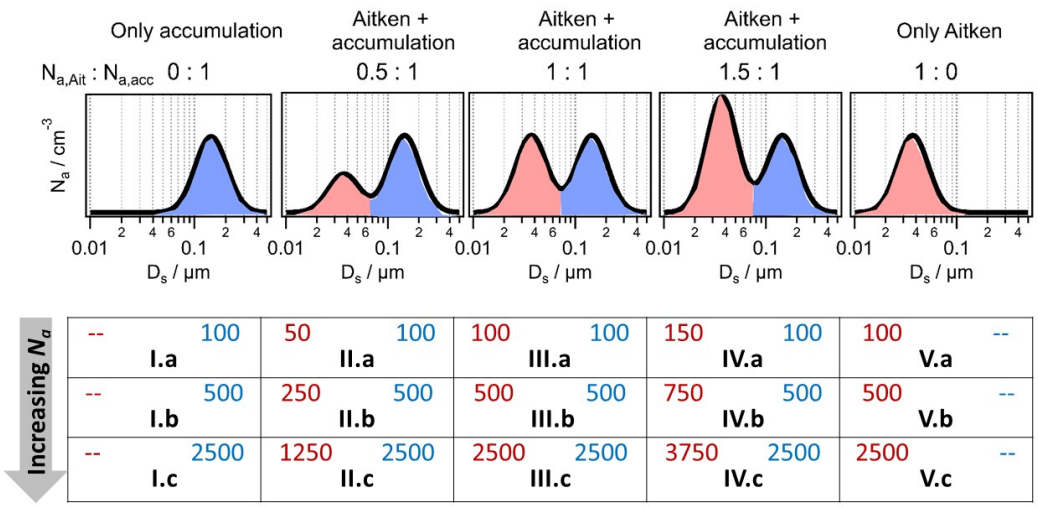

Figure 1. Schematic of model input aerosol size distributions (ASDs, designated I-V, a-c) with different number concentrations of Aitken mode particles ($N_{a,Ait}$, red) and accumulation mode particles ($N_{a,acc}$, blue). Particle number concentrations are given in units of cm^{-3}. The modal geometric mean diameters are $D_{g,Ait} = 0.037\,\mu$m and $D_{g,acc} = 0.145\,\mu$m .

2.2.2 Analysis of sensitivities $\xi(\kappa)$ and $\xi(N_a)$

Droplets are defined as particles with $D_{wet} \geq 3$ µm. This definition does not strictly follow Köhler theory that defines droplets as particles whose S_{crit} is exceeded. The reasoning for our definition is the comparability of model results to observational studies that commonly report data from cloud probes detecting particles above a fixed size threshold, e.g., Braga et al. (2021). As our study is intended to give guidance to future field and model studies, we use the size-based (3 µm) rather than the Köhler-based (D_{crit}) droplet definition. We define the smallest dry particle size on which droplets grow to $\geq 3\mu$m as D_{min}. The droplet number concentration N_d is calculated as the cumulative particle number concentration between D_{min} and the largest D$_(dry)$ (1.4 µm). We describe the predicted change in N_d as a function of particle hygroscopicity (κ) as the sensitivity

$\xi(\kappa)$:

$$\xi(\kappa) = \frac{\partial ln N_d}{\partial ln \kappa} \tag{E.4}$$

For comparison to conclusions on parameter regimes as discussed in previous model sensitivity studies, we also investigate the sensitivity of N_d to N_a

$$\xi(N_a) = \frac{\partial ln N_d}{\partial ln N_a} \tag{E.5}$$

These definitions follow the same approach as in previous model studies that investigated the sensitivity of N_d to κ and N_a for monomodal accumulation mode ASDs (e.g., McFiggans et al. (2006); Reutter et al. (2009); Ward et al. (2010); Pardo et al. (2019)).

Since N_d is predicted to increase above cloud base, we perform most of our sensitivity analyses at 20 m above the height level of maximum supersaturation (S_{max}). In a recent N_d closure study, we found not only best agreement of measured and predicted N_d at this height but also of the liquid water content, independently of the pollution level of the air mass (Braga et al., 2021).

3 Results and Discussion

3.1 Vertical profiles of N_d, D_{min} and $\xi(\kappa)$

Figure 2 shows the vertical profiles of N_d, D_{min} and $\xi(\kappa)$ as a function of κ (color-coding) for simulations with ASD I.b and ASD III.b at an updraft velocity of w = 2.9 m s^{-1}; complementary results for w = 1.0 m s^{-1} and 0.2 m s^{-1} are shown in Figures S1 and S2. The black lines denote the height, at which the supersaturation reaches its maximum value (Figure S3). At high w and κ, N_d shows significantly smaller N_d for the monomodal ASD I.b than for the bimodal ASD III.b (Figure 2a and b). The D_{min} values are nearly identical for the two ASDs for a given w (comparison of left and right columns in Figures 2, S1 and S2) and they are inversely correlated with N_d. Under these conditions, D_{min} reaches minimum values of $\sim$0.05 µm, which means that all accumulation mode particles form cloud droplets ($N_d \sim N_{a,acc}$ = 500 cm^{-3}) and N_d cannot further increase for ASD I.b. In the presence of an Aitken mode, a significant fraction of highly hygroscopic Aitken mode particles grow to cloud droplets ($N_d \sim$ 620 cm^{-3}, Figure 2b) as D_{min} is significantly smaller than the size range of the Hoppel minimum (D $\sim$0.07 µm).

The $\xi(\kappa)$ evolution for ASD I.b (Figure 2e) repeats the trends of D_{min} and mirrors those of N_d, i.e., $\xi(\kappa)$ is lowest for highest κ and w. For ASD I.b, $\xi(\kappa)$ reaches lowest values for the highest w when nearly all particles are grown to cloud droplets ($N_d \sim$ 500 cm^{-3}), and a decrease in D_{min} does not further increase N_d. The difference in $\xi(\kappa)$ for ASD I.b and III.b is significant (Figure 2e, f) as $\xi(\kappa)$ for the bimodal ASD III.b is predicted to increase for $\kappa >\sim$0.5 above the level of S_{max}. This inversion of $\xi(\kappa)$ occurs at the height, at which Aitken mode particles start contributing to N_d (Figure 2).While for the monomodal ASD I.b $\xi(\kappa)$ is predicted to continuously decrease with height, the increasing contribution of Aitken mode particles to N_d leads to the opposite trend, i.e. to highest $\xi(\kappa)$ values for particles with highest κ.

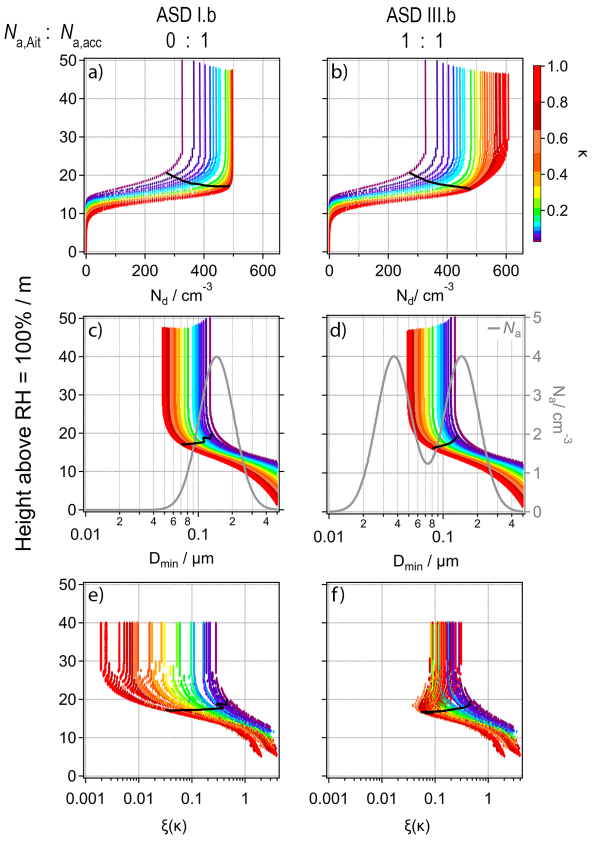

Figure 2. Vertical profiles of (a, b) cloud droplet number concentration (N_d), (c, d) dry size of smallest particles that contribute to N_d (D_{min}), overlaid by the corresponding ASD (grey lines), and (e, f) sensitivity of N_d to κ ($\xi(\kappa)$) for an updraft velocity w = 2.9 m s^{-1}. Left and right columns show results for ASD I.b and III.b, respectively. The black lines in all panels mark the height of S_{max} above the level of saturation (RH = 100%).

Generally, the differences in the vertical profiles for ASD I.b and III.b are smaller with lower w (Figures S1 and S2). At w = 1 m s^{-1}, N_d is only slightly lower for ASD I.b than for ASD III.b. The two modes overlap at the Hoppel minimum (Figure 1) and the small concentration of Aitken mode particles at this size explains the somewhat higher N_d in Figure S1 a as compared to Figure S1 b. At w = 0.2 m s^{-1}, only large accumulation mode particles are activated (activated fraction, $F_{act,acc} < \sim 0.5$ and $D_{min} \geq 0.12$ µm) and $\xi(\kappa)$ remains generally higher than for larger w. A high sensitivity implies that D_{min} is in a size range, in which the ASD exhibits a steep slope where a small change in D_{min} translates into a relatively large change in N_d.

Similar trends of $\xi(\kappa)$ with w were discussed in previous studies in which it was generalized that $\xi(\kappa)$ is highest at low w as only a small but significant fraction of the accumulation mode particles is activated (e.g., Moore et al. (2013); Ervens et al. (2005)). Reutter et al. (2009) showed low sensitivities of N_d at low w for very high N_a($\sim$ 10,000 cm^{-3}). In this case, the supersaturation is efficiently suppressed as the condensation term (Equation E.2) is dominated by N_a. As only very large

particles grow to droplet sizes, N_d would only include particles with D > $\sim$ 0.3 µm , i.e. only in a flat part of the ASD, where a small change in D_{min} does not lead to a significant change in N_d. The increased $\xi(\kappa)$ at high *w* for the bimodal ASD III.b (Figure 2f) follows the same reasoning as D_{min} is located at a size range where the Aitken mode exhibits approximately the same slope as at D_{min} for *w* = 0.2 m s^{-1}. For less hygroscopic particles, D_{min} is near the Hoppel minimum and thus $\xi(\kappa)$ is smaller than for high κ (Figure 3).

In all simulations, N_d is predicted to increase while D_{min} decreases until the air parcel reaches up to several tens of meters above the height level of S_{max} (Figures 2, S1, and S2), as particles continue to grow and eventually reach the size threshold of 3 µm. The size distributions of haze particles and droplets are shown in Figure S4 at four heights for the three *w* and κ = 0.04, 0.3 and 0.7; the red vertical lines indicate the size threshold (3 µm) for droplets. It can be seen that the separation of haze particles and droplets occurs at different heights, depending on κ and *w*. Hygroscopic Aitken mode particles successively grow at high *w* to similar droplet sizes as accumulation mode particles (orange box at the bottom of the figure), coinciding with the height at which $\xi(\kappa)$ increases. This $\xi(\kappa)$ trend is opposite to that for ASD I.b and also as found in previous studies of monomodal ASDs (Pardo et al., 2019; Cecchini et al., 2017) that showed decreasing sensitivities to aerosol properties with height.

If cloud droplets were defined based on D_{crit}, N_d would be computed at the level of S_{max} (black lines in Figures 2, S1, and S2) and remain constant above this height. This would result in different N_d as large haze particles may not be counted if their S_{crit} were not reached in cloud, and small particles whose S_{crit} is exceeded might also not be counted using our size-based droplet definition. Since N_d would not change above S_{max}, also $\xi(\kappa)$ would be constant above this level. A detailed comparison of predicted cloud properties applying the two droplet definitions (D_{crit} versus $D_{wet} \geq 2$ µm) was performed in a previous sensitivity study (Loftus, 2018). There it was shown that predicted N_d based on the two definitions show largest discrepancies at lowest *w* and/or high N_a, and that the droplet size distributions are generally narrower if droplets are defined based on D_{crit}. Also sensitivities would be overestimated if they are computed in the unstable bottom layer of the cloud at the level of S_{max}. It can be concluded that sensitivity studies, in which a droplet definition based on D_{crit} is applied will not only lead to higher absolute values of $\xi(\kappa)$ but at the same time, also to an underestimate of the sensitivity to κ as the predicted differences of $\xi(\kappa)$ for different κ values are much smaller (e.g., (Reutter et al., 2009)). Such studies might thus lead to biased conclusions if they are applied to ambient N_d measurements that are based on fixed size thresholds to discriminate cloud droplets.

3.2 Sensitivity to aerosol properties: $\xi(\kappa)$ and $\xi(N_a)$

3.2.1 Dependence of $\xi(\kappa)$ on D_{min} (ASD III.b)

In the following, we investigate more generally the parameter ranges, at which Aitken mode particles affect sensitivities and N_d in clouds. Our discussion will be limited to cloud conditions at a height of 20 m above S_{max}, i.e., when N_d has reached a constant value. Figure 3 shows results at 20 m above the levels of S_{max}. This height corresponds to $\sim$ 35 m above the level where RH = 100% in Figure 2e and f. Figure 3 depicts the $\xi(\kappa)$ values resulting from the 810 simulations for ASD III.b as a function of κ and *w*. The contour lines are color-coded by $0 \leq \xi(\kappa) \leq 1$. Parallel to the axes, six lines are marked for three κ

values (vertical lines at κ = 0.7 (orange), 0.3 (blue), and 0.04 (red)), and three updraft velocities (horizontal lines at w = 2.9 m s^{-1} (orange), 1.0 m s^{-1} (blue) and 0.2 m s^{-1} (red)).

Each $\xi(\kappa)$ can be related to a D_{min} (Figure 3). This relationship is shown in Figure 3b, where the $\xi(\kappa)$ values along the vertical lines are overlaid by the aerosol size distribution. Figure 3c shows the D_{min} range that is covered by the simulations for the three constant κ values. The end points of the D_{min} ranges in Figure 3b and c are connected by vertical dashed lines. In the same way, Figure 3d shows D_{min} for $\xi(\kappa)$, i.e. along the horizontal lines in Figure 3a.

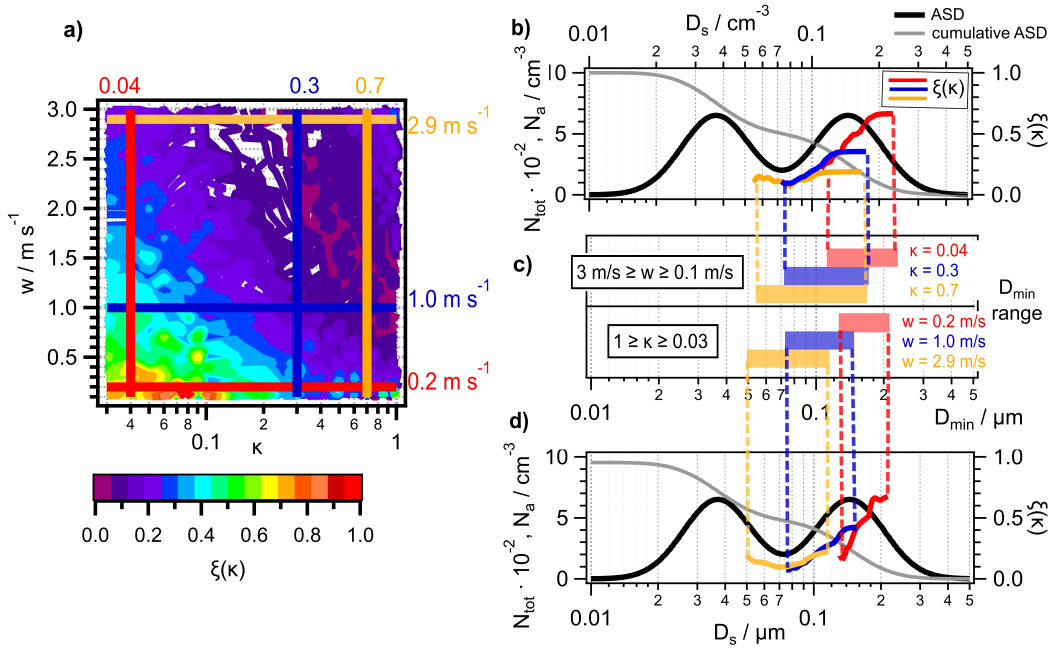

Figure 3. a) Sensitivity of cloud droplet number concentration to aerosol hygroscopicity ($\xi(\kappa)$) as a function of κ and w for ASD III.b at 20 m above S_{max}. b): $\xi(\kappa)$ (right axis) as a function of D_{min} for κ = 0.04 (red), κ = 0.3 (blue), and κ = 0.7 (orange). c) Ranges of D_{min} for the simulations in panel b) and d). b): $\xi(\kappa)$ (right axis) as a function of D_{min} for w = 0.2 m s^{-1} (red), w = 1.0 m s^{-1} (blue), and w = 2.9 m s^{-1} (orange).

In line with the results in Figures 2, $\xi(\kappa)$ and D_{min} are highest for small κ and w and decrease with increasing w (Figure 3a and b). Analogous trends are shown in Figure 3b for the $\xi(\kappa)$ values as a function of D_{min} along the horizontal lines (constant w) in Figure 3a. The $\xi(\kappa)$ lines for the three κ or three w values, respectively, overlap as $\xi(\kappa)$ depends on the slope of the ASD at D_{min}. Different combinations of κ and w can result in identical D_{min} values and thus yield the same $\xi(\kappa)$ values (contour lines of identical color in Figure 3a). When D_{min} is near the Hoppel minimum, a change in D_{min} by either of the parameters does not lead to a significant change in N_d leading to low $\xi(\kappa)$ values. Accordingly, $\xi(\kappa)$ increases when D_{min} reaches sizes smaller than the Hoppel minimum.

Overall, $\xi(\kappa)$ as a function of D_{min} traces the shape of the ASD (black line in Figure 3a and c). The combinations of *w* and κ for which an increase in $\xi(\kappa)$ with a decrease in D_{min} is predicted are those in the upper right corner of Figure 3a.

The D_{min} ranges, covered by a variation of *w* or κ by the same factor ($\sim$ 30) (colored bars in 3b), are similar. This suggests that an equal change in either of the parameters affects D_{min} to the same extent. However, this relationship cannot be generalized. Figures S5 and S6 show equivalent results to those in Figure 3, but for N_a = 200 cm^{-3} and N_a = 5000 cm^{-3}, respectively. Smaller N_a implies a smaller condensation term (Equation E.2), resulting in a higher supersaturation, which allows also smaller particles to grow to cloud droplets. Thus, for N_a = 200 cm^{-3}, the D_{min} ranges are shifted to smaller values, resulting in higher activated fractions (Figure S5b and c). Accordingly, the D_{min} ranges move to larger values for N_a = 5000 cm^{-3} (Figure S6b and c).

While for N_a = 200 cm^{-3} and 1000 cm^{-3} the minima in the $\xi(\kappa)$ curves coincide with the Hoppel minimum of the ASD, the minimum of $\xi(\kappa)$ is shifted to somewhat larger sizes for N_a = 5000 cm^{-3} (Figure S6). At such high N_a, the supersaturation is very low (Figure S7). Under these conditions, an increase in *w* or κ might result in only small changes in N_d because of buffering effects, i.e. the growth of additional droplets suppresses the supersaturation and prevents further activation.

The comparison of Figures 3, S5 and S6 reveals that not only the ranges of D_{min} values are shifted as a function of N_a, but also that their widths differ depending on N_a. The D_{min} ranges are widest for N_a = 200 cm^{-3} which implies that for these conditions N_d is most sensitive to κ and *w*, as a change in these parameters causes a significant change in D_{min} and N_d. Correspondingly, for N_a = 5000 cm^{-3}, a change in *w* or κ only leads to a small change in D_{min}. While such a shift in D_{min} only leads to small change in the activated fraction, it translates into a relatively large difference in N_d, resulting in high $\xi(\kappa)$.

This analysis demonstrates that the similarity in the D_{min} ranges in Figure 3b and c resulting from a change in κ or *w* by the same factor are coincidental and should not be generalized to all conditions as the relative sensitivities to κ and *w* depend on N_a. However, it also shows that conditions exist under which N_d is similarly sensitive to *w* and κ and both parameters need to be taken into account to accurately predict N_d.

3.2.2 Sensitivity regimes of $\xi(N_a)$ for mono- and bimodal ASDs

Previously, sensitivity of N_d to N_a and to *w* were presented in terms of aerosol (N_a)- and updraft (*w*)-limited regimes (Reutter et al., 2009, 2014; Chang et al., 2015). The N_a-limited regime is characterized by high activated fractions, i.e., when an increase in N_d can only be caused by an increase in N_a and N_d depends linearly only on N_a; the *w*-limited regime occurs for small activated fractions where an increase in *w* leads to sufficient decrease in D_{min} to increase N_d. Our analysis in Section 3.2.1 suggests that for wide parameter ranges, N_d is similarly sensitive to κ and *w*. To discuss these results in the context of N_a- and *w*-limited regimes, we explore the sensitivity of N_d to N_a, $\xi(N_a)$, as a function of *w* for κ = 0.7 for ASD I, III and V with 500 cm^{-3} $\leq N_a \leq$ 5000 cm^{-3}. Figure 4a shows N_d for ASD I as a function of N_a and *w* and confirms the thresholds between the regimes as suggested by Reutter et al. (2009), i.e., N_a-limitation above $w/N_a > \sim 10^{-3}$ m s^{-1} cm^3 and *w*-limitation below $w/N_a < \sim 10^{-4}$ m s^{-1} cm^3, with a transitional regime in-between. Accordingly, $\xi(N_a)$ approaches unity in the N_a-limited regime when nearly all particles are activated (upper left corner of Figure 4b) and even exceeds this value at high N_a and low *w* (bottom right corner).

The $\xi(Na)$ pattern in Figure 4d exhibits a minimum when the activated fraction is ~0.7. This fraction corresponds to the size range at which the cumulative ASD exhibits the largest slope. If more particles are activated, the relative change in N_d and therefore in $\xi(Na)$ become smaller.

In the presence of an Aitken mode, in addition to an accumulation mode (ASD III; Figure 4c), N_d is not limited by $N_{a,acc}$ under the same N_a and w conditions as for ASD I since only a small fraction of the Aitken mode is activated. Figure 4d shows the same $\xi(N_a)$ patterns as the part of Figure 4b for $N_a \leq 2500$ cm^{-3} under conditions where only accumulation mode particles are activated and thus contribute to N_d and to $\xi(N_a)$. Thus, the transitional regime is extended to a broader parameter space as $\xi(N_a)$ does not show a constant value of unity as it should in an N_a-limited regime. As at high N_a and low w, only accumulation mode particles contribute to N_d, the contours for the w-limited regime do not differ between Figures 4b and d.

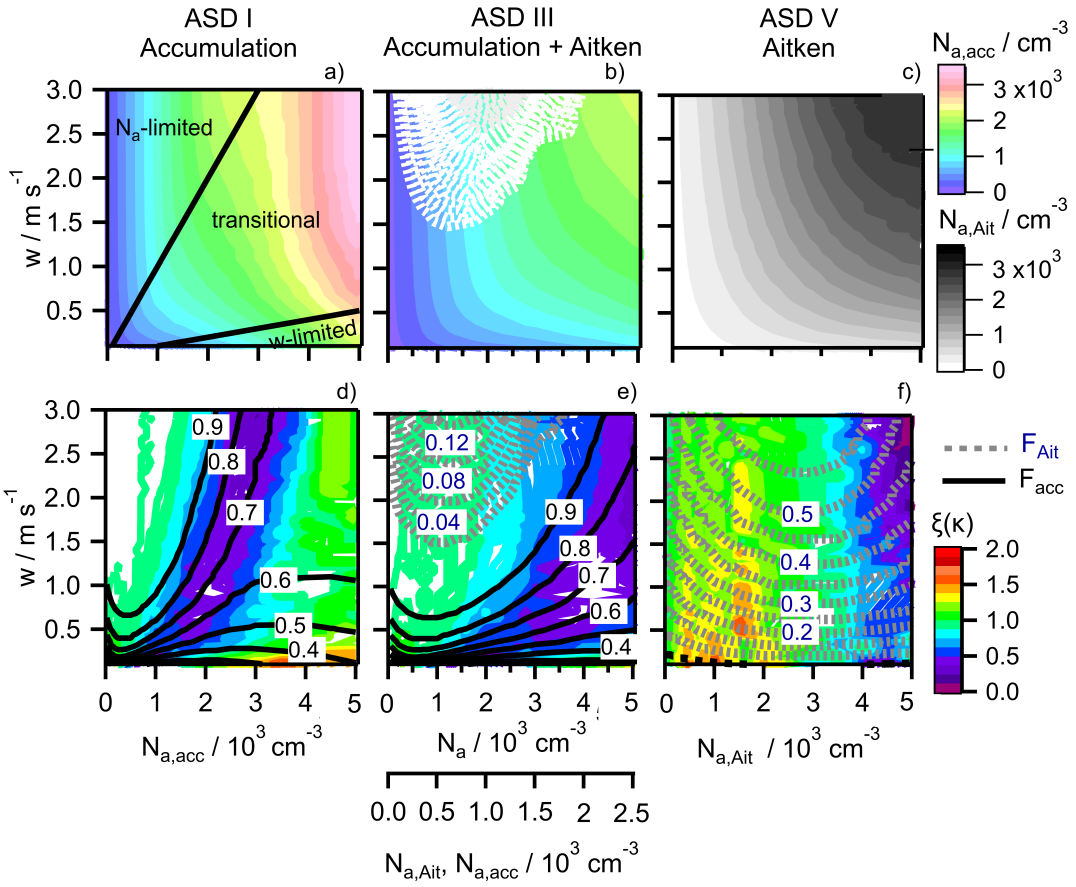

Figure 4. Upper panels: N_d as a function of w and N_a for ASD and κ = 0.7. a) I, c) III and e) V. Color scale: $N_{d,acc}$, black/white scale: $N_{d,Ait}$. Bottom panels: Corresponding $\xi(N_a)$ for ASD b) I, d) III and f) V. Solid black lines show contours of activated fraction of the accumulation mode ($F_{act,acc}$), dashed grey lines show contours of activated fraction of the Aitken mode ($F_{act,Ait}$).

For the monomodal ASD V (Aitken mode), the activated fraction reaches at most ∼0.6 (Figure 4e, f); thus, the aerosol-limited regime is not reached. However, for N_a >∼1000 cm^{-3} and w < ∼1.0 m s^{-1}, N_d is linearly dependent on w and independent of N_a, which implies a w-limited regime for w/N_a < ∼10^{-3} m s^{-1} cm^3, i.e. shifted by an order of magnitude as compared to ASD I. Accordingly, $\xi(N_a) \geq 1$, similar to the $\xi(N_a)$ values reached for much higher $N_{a,acc}$ and lower w for the monomodal accumulation mode ASD I. The $\xi(N_a)$ pattern in Figure 4b exhibits a minimum when the activated fraction is ∼0.7. This fraction corresponds to the size range at which the cumulative ASD has the largest slope. If more particles are activated, the relative change in N_d and therefore in $\xi(N_a)$ become smaller. In summary, based on these trends of $\xi(N_a)$ and those of $\xi(\kappa)$ in Section 3.2.1, the following conclusions can be drawn:

- The N_a and w-limited regimes are dependent on particle size and thus the w/N_a limits are different for monomodal Aitken vs accumulation mode ASDs and also for monomodal vs bimodal ASDs.
- The sensitivities of N_d to ASD parameters (N_a, D_g, κ) and to w depend on their value combinations.
- Under most w and N_a conditions as considered here for bimodal ASDs, the N_a-limited regime is not reached, as they cover the transitional regime.
- The equivalency of a change in w and κ to affect D_{min} (Figure 3) implies that a κ-sensitive regime could be equally defined and taken into account as a w-sensitive regime when exploring sensitivities of N_d.

3.2.3 Sensitivities $\xi(\kappa)$ for different aerosol size distributions

The parameter ranges of w, κ and N_a considered in our simulations in the presence of an Aitken mode constrain transitional or w-limited regimes, in which N_d can be equally influenced by w and κ. Therefore, we explore in detail the w,κ combinations, above which Aitken mode particles significantly affect N_d and $\xi(\kappa)$. Figure 5 shows $\xi(\kappa)$ contour plots for all cases as defined in Figure 1; the middle column (ASD III) repeats Figures 3a, S5a and S6a. As the supersaturation and activated fractions are closely related to $\xi(\kappa)$, the corresponding figures for the 15 cases are shown in Figures S7 and S8.

The $\xi(\kappa)$ values for the monomodal accumulation mode ASD I are shown in the first column of Figure 5 (a: N_a = 100 cm^{-3}, b: 500 cm^{-3} and c: 2500 cm^{-3}). The white regions in the upper right part of the figures mark the parameter spaces above which $\xi(\kappa)$ ∼0, i.e., the N_a-limited regime. At high N_a, this space is shifted to higher κ and w, in agreement with the trends of larger D_{min} at higher N_a (Section 3.1.1). The trends in $\xi(\kappa)$ along Columns II, III and IV show the effect on $\xi(\kappa)$ due to increasing $N_{a,Ait}$ / $N_{a,acc}$ (0.5, 1.0, 1.5) for a fixed $N_{a,acc}$ in each row. The $\xi(\kappa)$ contours in the parameter space, at which only accumulation mode particles contribute to N_d do not significantly change for a given $N_{a,acc}$ (bottom left corners of panels ASD I - IV). However, with increasing $N_{a,Ait}/N_{a,acc}$, the absolute $\xi(\kappa)$ values increase, i.e., ∼0.15 $\lesssim \xi(\kappa) \lesssim$0.25 for the major part of panels IV.a and IV.b whereas $0 \leq \xi(\kappa) \lesssim$0.25 in panels II.a and II.b. A higher $N_{a,Ait}/N_{a,acc}$ causes the range to narrow, at which $\xi(\kappa)$ shows a minimum, while the w,κ combinations for minimum $\xi(\kappa)$ are not significantly shifted (ASD I - IV within a each row in Figure 5). This trend in $\xi(\kappa)$ is caused by the higher $N_{a,Ait}$ near the Hoppel minimum with increasing $N_{a,Ait}/N_{a,acc}$, and thus higher N_d when D_{min} ∼0.07 µm.

At the highest N_a, the $\xi(\kappa)$ patterns do not show any significant difference (I.c to IV.c in Figure 5). As under these conditions for κ, w and N_a only accumulation mode particles are activated, the presence of the Aitken mode does not affect $\xi(\kappa)$ within the κ and w ranges considered here. If our scales were extended to updraft velocities of several meters per second as encountered in deep convective clouds, Aitken mode particle particles may activate even if $N_{a,acc} \geq 2500$ cm^{-3} resulting in similar contour patterns as for lower N_a and the w ranges considered here. However, in polluted air masses eventually a saturation effect in terms of droplet formation is reached above which N_d and effective radii do not significantly change as it was shown for convective clouds in the Amazon region (Polonik et al., 2020).

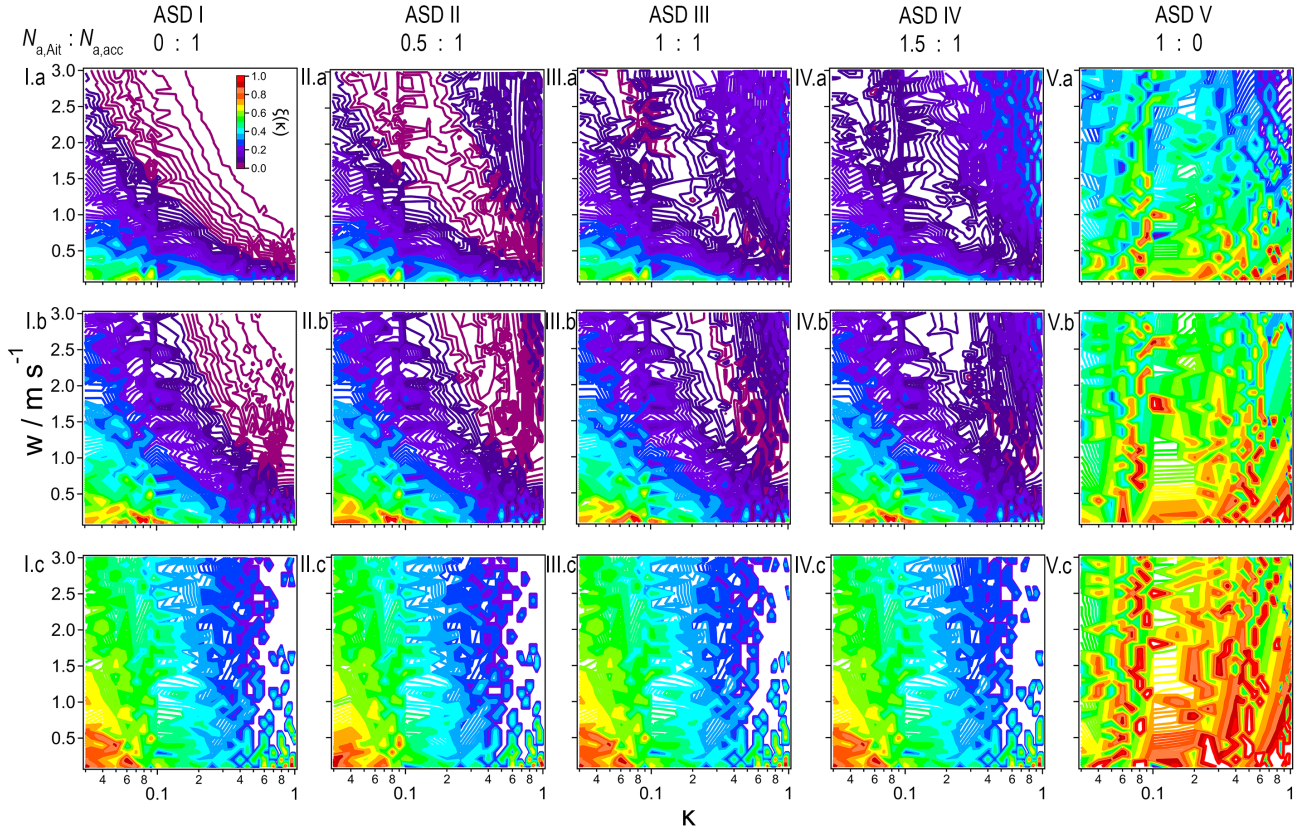

Figure 5. Sensitivity of N_d to κ ($\xi(\kappa)$) as a function of w and κ for ASDs I.a - V.c (Figure 1). Contour plots ($0 \leq \xi(\kappa) \leq 1$, color-code in panel a) are based on 810 model simulations assuming 30 different values of w and 27 different values of κ for each ASD. Column ASD III repeats panels a) in Figures 3, S5 and S6.

At first sight, the $\xi(\kappa)$ patterns for ASD V are very different to those of the other ASDs (columns I-IV vs V in 5). These apparently different trends can be reconciled based on the discussion in Sections 3.2.1. and 3.2.2: The higher $\xi(\kappa)$ for highly hygroscopic particles (red area at the bottom right corner in Figure 5V.a-c) implies that at low w, a large number of particles with high κ form droplets whereas N_d is smaller for less hygroscopic particles. This suggests that D_{min} for high κ is located

in a 'steep' part of the ASD with relatively high $N_{a,Ait}$, and a decrease in κ increases D_{min} such that it is in the flat part of the ASD ($D \sim 0.1$ µm).

For ASD I, such situations are not encountered for the chosen parameter ranges. Even for the lowest κ and *w*, a significant fraction of $N_{a,acc}$ is activated, and any change in D_{min} due to a change in *w* or κ shifts it along the 'steep part' of the cumulative ASD. If we performed simulations for higher $N_{a,acc}$, i.e., for conditions typical for a *w*-limited regime, D_{min} would be shifted to even larger sizes than shown in Figure S6 b and c, resulting in very small N_d and $\xi(\kappa)$.

As discussed in Section 3.2.2., the conditions for ASD V can be described as a *w*- and/or κ-limited regime that it is characterized by a relatively low w/Na (or κ/N_a) ratio. Using ASD I, similar $\xi(\kappa)$ patterns as in Figure 5V.a could be obtained using ASD I.a for smaller κ and/or *w* or higher N_a than considered here. This can be seen in the upper row of Figure 5 where panel V.a is apparently a continuation of panel I.a to smaller κ values. However, the match of the corresponding panels (V.b to I.b or V.c to I.c, respectively) is not as perfect which suggests different sensitivities of $\xi(\kappa)$ to D_g and κ, depending on N_a. Thus, not only are the limits of the *w*-limited regime depending on D_g (i.e., accumulation or Aitken mode) but also the parameter ranges that characterize the regimes.

The comparison of the influence on $\xi(\kappa)$ due to increasing $N_{a,Ait}$ (V.a, b, c in Figure 5) and on $\xi(N_a)$ (Figure 4f) shows that $\xi(\kappa)$ is increasing whereas $\xi(N_a)$ is decreasing. Therefore, when high concentrations of Aitken mode particles dominate the ASD, N_d is highly sensitive to κ and *w*, and less to $N_{a,Ait}$. While in the presence of accumulation-mode-dominated ASDs such *w*- and κ-sensitive conditions might be only encountered in highly polluted air masses (e.g., biomass burning), they can occur for Aitken mode dominated ASDs at much lower aerosol concentrations. This shift in sensitivities might partially explain the large uncertainties in cloud properties predicted in global model studies when Aitken mode particles significantly influence N_d and other cloud properties, e.g., (Lee et al., 2013; Chang et al., 2021).

3.3 Dependence of $\xi(\kappa)$ on κ_{acc} and D_g

3.3.1 Influence of constant κ_{acc} on $\xi(\kappa)$

While we have assumed so far that both Aitken and accumulation modes have the same κ, such conditions are rarely encountered in the atmosphere. They might occur, for example, when sea-salt contributes significantly to both modes (Wex et al., 2016). However, more frequently the accumulation mode consists of material of higher hygroscopicity as it accumulates sulfate and other compounds during cloud processing and other ageing processes. Continental accumulation modes typically exhibit values in a range of $0.1 < \kappa_{acc} \lesssim 0.5$ with an average value of $\kappa_{acc} \sim 0.3$ (Andreae and Rosenfeld, 2008). The Aitken mode is comprised of fresher, less hygroscopic particles with $0 < \kappa \lesssim 0.05$ in urban and continental air masses, corresponding to hygroscopic growth factors ≤ 1.1 at RH = 90 %. Aged Aitken mode particles are more hygroscopic, with $\kappa \sim 0.3$ in the free troposphere and $\kappa \sim 0.6$ in remote marine air (McFiggans et al., 2006). Similar trends in the hygroscopicity of the two modes were also observed during the wet season in the Amazon with $\kappa_{Ait} \sim 0.1$ and $\kappa_{acc} \sim 0.2$ (Zhou et al., 2002; Gunthe et al., 2009). In a global model study, fairly large differences were predicted above oceans ($\kappa_{Ait} \sim 0.5$, $\kappa_{acc} \sim 1$), and more similar values for both modes above continents ($\sim 0.3 \leq \kappa \lesssim 0.8$; Chang et al. (2017)).

To explore situations with $\kappa_{acc} \neq \kappa_{Ait}$, we repeat the simulations for ASD III.b but use a single value of κ_{acc}, whereas the full range of $0.02 \leq \kappa_{Ait} \leq 1$ is applied (Figure 6a). For low w and κ, $\xi(\kappa_{Ait})$ is zero (white space in Figure 6c and d) because in this parameter range droplets only form on accumulation mode particles and a change in κ_{Ait} does not affect N_d. When κ_{Ait} > κ_{acc}, small accumulation mode particles may not become activated whereas more hygroscopic (but smaller) Aitken mode particles sufficiently grow and contribute to N_d. Thus, the total N_d is the sum based on two separate D_{min} values for Aitken and accumulation modes, respectively. The activated fractions for the two simulations are compared in Figure S8; $F_{act,acc}$ appears as horizontal lines as it is independent of κ_{Ait}; only at high κ_{Ait} values, there are small deviations from this behavior as very hygroscopic Aitken mode particles may sufficiently suppress the supersaturation and prevent efficient growth of accumulation mode particles. The large overlap of the activated fractions from both modes in Figure S8 a (κ_{acc} = 0.1) demonstrates that at $w \gtrsim$1 ms^{-1}, large Aitken mode particles with $\kappa_{Ait} \gtrsim 0.3$ may grow to droplet sizes even though only ∼70% of accumulation mode particles are activated whereas the smallest 30% of the accumulation mode particles have not been activated yet.

The similar $\xi(\kappa_{(Ait)})$ values in Figure 6b-d show their weak dependence on κ_{acc}. The supersaturation is largely controlled by $N_{a,acc}$ resulting in very similar values over the full κ range, independent of the presence of an Aitken mode (Figure S7 I.b - IV.b). When κ_{acc} = 0.1, droplet formation on Aitken mode particles occurs for slightly lower values of κ and w as compared to the case with κ_{acc} = 0.5 (Figure 6c and d). More hygroscopic accumulation mode particles efficiently suppress the supersaturation and prevent smaller (Aitken mode) particles from efficient growth. Thus, for the same w,κ combinations, $F_{act,Ait}$ is smaller when κ_{acc} = 0.5 compared to κ_{acc} = 0.1 (Figure S8).

Similar feedbacks of the two modes on cloud properties were described in previous model sensitivity studies that showed more Aitken mode particles to activate in the presence of less hygroscopic accumulation mode particles (Kulmala et al., 1996). In the latter study, soluble and insoluble mass fractions were used as proxies of particle composition, and it was shown that CCN activation can be parameterized by the soluble mass, which may be higher in large, soluble (hygroscopic) Aitken than in small, less soluble accumulation mode particles. A significant contribution of Aitken mode particles to N_d (> 50%) was observed at a background site in northern Finland with average activated fractions of $F_{act,acc}$ ∼87% and $F_{act,Ait}$ ∼30% (Komppula et al., 2005). While such observations could be equally explained by externally mixed aerosol, this would result in the same effects during cloud processing: Efficient formation of mass (e.g. sulfate) in droplets formed on Aitken mode particles that lead to a narrowing of the Hoppel minimum rather than to a widening. In a global model study, it was demonstrated that efficient sulfate formation in such droplets could contribute several percent ($\gtrsim$5%) to the global sulfate budget (Roelofs et al., 2006).

3.3.2 Influence of $D_{g,Ait}$ and $D_{g,acc}$ on $\xi(\kappa)$

The parameters commonly used to characterize lognormal ASDs, D_g and σ_g, were identified as the most important aerosol parameters in affecting cloud properties (e.g., Feingold (2003); Ervens et al. (2005); Reutter et al. (2009); Ward et al. (2010); Anttila et al. (2012)). To compare their importance for accumulation and Aitken modes, we vary $D_{g,Ait}$ and $D_{g,acc}$ within the range of observed values. Our base case values ($D_{g,Ait}$ = 0.037 µm, $D_{g,acc}$ = 0.145 µm, Figure 1) are typical for oceanic aerosol (Wex et al., 2016). In addition, we apply $D_{g,acc}$ = 0.13 µm and 0.17 µm for continental aerosol (Pöhlker et al., 2016, 2018). The size of Aitken mode particles strongly depends on their ageing state; it is larger for continental aerosol than above

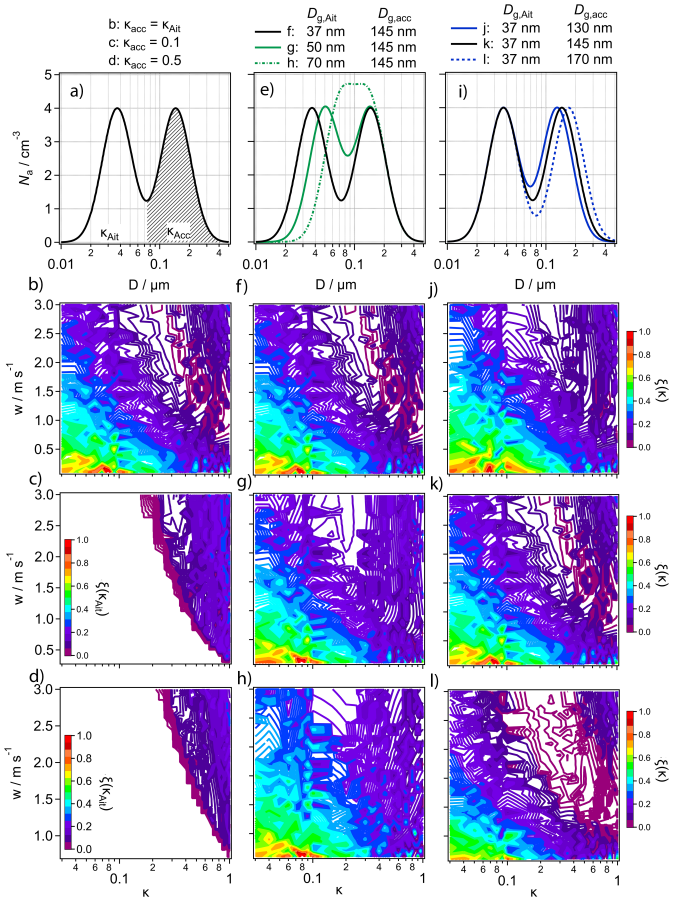

Figure 6. Sensitivity of N_d to κ ($\xi(\kappa)$) as a function of w and κ for variable ASDs and aerosol properties as outlined in the top panels. a) Schematic ASD with constant κ_{acc}; b) identical to Figure 5 III.b, c) $\xi(\kappa_{Ait}$, assuming κ_{acc} = 0.1, d) $\xi(\kappa_{Ait}$, assuming κ_{acc} = 0.5, e) ASDs with different $D_{g,Ait}$ in addition to ASD III, f) identical to Figure 5 III.b, g) $\xi(\kappa)$ for $D_{g,Ait}$ = 0.05 µm, h) $\xi(\kappa)$ for $D_{g,Ait}$ = 0.07 µm, i) ASDs with different $D_{g,acc}$ in addition to ASD III, j) $\xi(\kappa)$ for $D_{g,acc}$ = 0.13 µm, k) identical to Figure 5 III.b, l) $\xi(\kappa)$ for $D_{g,acc}$ = 0.17 µm

the ocean (e.g., Birmili et al. (2001); Heintzenberg et al. (2004); Pöhlker et al. (2016, 2018)). In sensitivity tests, we assume $D_{g,Ait}$ = 0.05 µm and 0.07 µm while keeping $D_{g,acc}$ = 0.145 µm.

We use ASD III.b as the reference case; it is shown together with the D_g-shifted ASDs in Figure 6e and i. The panels below the ASDs show the effect on $\xi(\kappa)$ of increasing $D_{g,Ait}$ (f, g, h) and $D_{g,acc}$ (j, k, l). With increasing $D_{g,Ait}$, the parameter space at which $\xi(\kappa)$ exhibits minimum values is shifted to lower w and κ values. The lowest values of $\xi(\kappa)$ (~0) are predicted for the smallest $D_{g,Ait}$ whereas $\xi(\kappa)$ ~0.2 for most of the w,κ space above which Aitken mode particles are activated. This is in agreement with our interpretation of Figure 3 that the dependence of $\xi(\kappa)$ on D_{min} traces the ASD shape. With $D_{g,Ait}$ = 0.07 µm, there is no w,κ space, in which $\xi(\kappa)$ shows a distinct minimum as both modes largely overlap (green dotted line

in Figure 6e). As D_{min} is determined by the supersaturation, which, in turn, is largely controlled by the accumulation mode properties ($N_{a,acc}$, $D_{g,acc}$, κ_{acc}), a shift of $D_{g,Ait}$ to larger sizes moves D_{min} to a different part of the ASD. For example, while $D_{min} \sim 0.06$ µm only leads to a small activated fraction of Aitken mode particles ($F_{act,Ait} < 0.1$) if $D_{g,Ait} = 0.037$ µm, it would be > 0.5 with $D_{g,Ait} = 0.07$ µm.

Accordingly, the trends in $\xi(\kappa)$ for a change in $D_{g,acc}$ (Figure 6j, k, l) can be explained: The Hoppel minimum is widest for the ASD with $D_{g,acc} = 0.17$ µm which is reflected by the large space, in which $\xi(\kappa) \sim 0$ (Figure 6l). However, unlike the shift of the range in which $\xi(\kappa)$ shows a minimum to lower *w*,κ values for increasing $D_{g,Ait}$, the *w*,κ space becomes only broader for larger $D_{g,acc}$ but barely changes its position. It can be concluded that $D_{g,acc}$ is of minor importance as compared to $D_{g,Ait}$ for the *w*,κ parameter space above which Aitken mode particles contribute to N_d.

4 Updraft and hygroscopicity regimes of Aitken mode CCN activation

Our sensitivity studies have shown that for bimodal (Aitken and accumulation mode) ASDs, the *w*,κ combinations resulting in $\xi(\kappa)$ minimum values can be used as a criterion of conditions under which Aitken mode particles contribute to N_d. An increase in *w* or κ decreases D_{min} to sizes smaller than the region of the Hoppel minimum.

To provide a general framework of our model results, we extract from the sensitivity simulations the *w*,κ combinations where $F_{act,Ait} = 0.05$ as a threshold, above which Aitken mode particles may significantly contribute to the total droplet number concentration. Figure 7a and c presents a selection of our model ASDs, together with additional ASDs ($N_{a,Ait}/N_{a,acc} \sim 10$ and ~0.1) to further map out the parameter space. In the bottom panels, the *w*,κ lines are summarized from each simulation that correspond to $F_{act,Ait} = 0.05$ (Figure 7b, d).

The black lines in Figure 7 show two ASDs with equal contributions of Aitken and accumulation mode to N_a (1000 cm^{-3}, ASD III.b). For ASDs of these D_g and N_a, any combination along the lines yields $F_{act,Ait} \geq 0.05$, such as $w \geq 1.5$ m s^{-1} and $\kappa_{Ait} \sim 1$, or $\kappa \geq 0.3$ and $w \sim 3$ m s^{-1}, respectively. The red lines in Figure 7b mark the shift of the *w*,κ as a function of N_a and $N_{a,acc}/N_{a,Ait}$: Decreasing N_a of both modes by a factor 5 moves the line to much lower *w* and κ values, such that Aitken mode particles with $\kappa \sim 0.4$ may be activated at $w \gtrsim 1$ m s^{-1} and more hygroscopic Aitken mode particles at even lower *w* (red dotted line). When the ASD is dominated by an Aitken mode ($N_{a,Ait} \sim 10 N_{a,acc}$), Aitken mode particles with $\kappa_{Ait} \geq 0.1$ will be activated at $w \geq 1$ m s^{-1} (red dashed line). Conversely, when $N_{a,acc} \sim 10 N_{a,Ait}$ with $N_{a,Ait} = 55$ cm^{-3}, the *w* and κ values are nearly outside the ranges of our κ and *w* scales (red solid line). Results for even higher N_a (2500 - 6750 cm^{-3}) are consequently not included in the figure because under these conditions, the efficient suppression of the supersaturation by the high $N_{a,acc}$ prevents Aitken mode particles from being activated within the considered parameter ranges of *w* and κ. Obviously, for wider *w* ranges as relevant for pyrocumuli or other highly convective cloud systems, corresponding thresholds and *w*,κ combinations could be derived on extended axes.

The purple lines in 7c correspond to results for constant $N_{a,acc} = 500$ cm^{-3} and for $N_{a,Ait}$ being 0.5 and 1.5 times that of the accumulation mode (ASD II.b, IV.b). The fact that they do not show any noticeable difference to results using ASD III.b

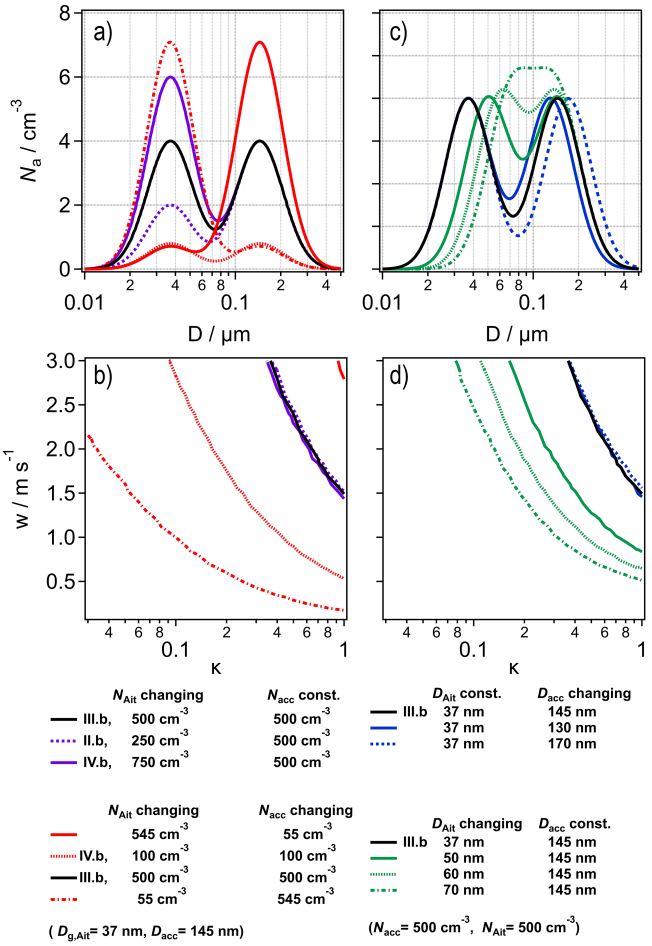

Figure 7. Updraft and hygroscopicity regimes where Aitken mode particles are relevant as CCN. a) Aerosol size distributions with different N_a and $N_{a,Ait}$ / $N_{a,acc}$, b) Lines indicate the w, κ combinations for which $F_{act,Ait}$ = 0.05 using the corresponding ASDs in a) (same color), c) Aerosol size distributions with different $D_{g,Ait}$ and $D_{g,acc}$, d) Lines indicate the w, κ combinations for which $F_{act,Ait}$ = 0.05 using the corresponding ASDs in c) (same color).

demonstrates that the ratio $N_{a,Ait}/N_{a,acc}$ - if $N_{a,acc}$ is approximately constant - does not significantly impact the position of the w,κ line.

In Figure 7d, we show the effects of $D_{g,Ait}$ and $D_{g,acc}$ on the w,κ space. A change in $D_{g,acc}$ from 0.145 µm to 0.13 µm or
415 to 0.17 µm has a negligible effect (blue solid and dotted lines). The low sensitivity of the w,κ line position to $D_{g,acc}$ suggests that it is applicable to continental and marine air masses, largely independent of $D_{g,acc}$. However, an increase in $D_{g,Ait}$ from 0.037 µm (ASD III.b) to 0.05 µm, 0.06 µm and 0.07 µm (green lines) significantly reduces the w and κ values that are required to activate Aitken mode particles. Thus, ageing processes might efficiently increase $D_{g,Ait}$ to those of CCN.

Figure 7b and d represents a simple scheme that can be applied to estimate whether Aitken mode particles contribute to N_d under ambient conditions in various air masses and cloud types. While we did not explore all relevant combinations of the parameters that are commonly used to characterize ASDs (N_a, $N_{a,Ait}/N_{a,acc}$, $D_{g,acc}$, $D_{g,Ait}$), the ranking of their relative importance in determining the position of the *w*,κ line is expected to hold generally true.

5 Summary and conclusions

Previous field and model studies suggested that not only accumulation, but also - under specific conditions - Aitken mode particles increase cloud droplet number concentrations and be involved in aerosol-cloud interactions. However, the conditions, under which the Aitken mode significantly contributes to cloud droplet number concentration (N_d) had not been fully constrained.

Using an adiabatic parcel model, we systematically investigated the conditions under which Aitken mode particles contribute to N_d for wide ranges of aerosol size distribution (ASD) parameters (particle number concentrations of accumulation and Aitken modes, $N_{a,acc}$, $N_{a,Ait}$, mode diameters, $D_{g,acc}$, $D_{g,Ait}$, and hygroscopicities κ_{acc}, κ_{Ait}), and of the updraft velocity *w* for N_d. In previous model sensitivity studies of monomodal ASDs, aerosol - and updraft -limited regimes were defined in which N_d depends linearly on N_a or *w* (Reutter et al., 2009). Using this concept, we show that Aitken mode particles are not activated if updraft-limited conditions prevail in the presence of a dominant accumulation mode (high $N_{a,acc}$). Also aerosol-limited conditions do not occur as by far not all Aitken mode particles are activated (for w $\leq$ 3 ms^{-1}, i.e., updraft velocities of abundant cloud types) and thus the transitional regime (between Na and *w* limitations) exists over wider parameter spaces than in the presence monomodal accumulation mode ASDs. When ASDs are dominated by an Aitken mode, we find that N_d is highly sensitive to *w* even at low $N_{a,Ait}$ which implies that the *w*/N_a regime limits as identified previously for accumulation mode ASDs are not always applicable, but they depend on parameter value combinations of D_g, N_a, κ and *w*.

Exceeding the previous framework that was restricted to *w* and N_a-limitations, we show that the sensitivities of N_d in the transitional and *w*-limited regimes equally depend on *w* and κ. Therefore, we explored in detail the sensitivity of N_d to κ, $\xi(\kappa)$, as a function of *w* for ASDs that differ in the number of modes (mono- or bimodal), $N_{a,Ait}/N_{a,acc}$ and total N_a. Based on the patterns of $\xi(\kappa)$ as a function of *w* and κ, we analyse the dependence of the *w*,κ range, above which Aitken mode particles contribute to N_d on the ASD parameters. We show that $\xi(\kappa)$ exhibits minimum values for *w*,κ combinations for which the smallest activated particle size (D_{min}) is near the Hoppel minimum and increases when smaller Aitken mode particles are activated. Defining lines near these *w*,κ combinations as the minimum threshold , it can be estimated under which aerosol (N_a, κ, D_g) and *w* conditions Aitken mode particles start contributing to N_d. We conclude that the most important requirements are a low number concentration of total and accumulation mode particles (N_a, $N_{a,acc}$) and/or a large mode diameter of the Aitken mode ($D_{g,Ait}$). While this ranking repeats previous findings for sensitivities to monomodal ASDs (e.g., Ervens et al. (2005); Reutter et al. (2009); Ward et al. (2010); Cecchini et al. (2017); Pardo et al. (2019)), our analysis exceeds these studies as it evaluates the relative importance of these parameters of accumulation and Aitken modes for the activation of Aitken mode particles.

Applying this framework to typical ambient aerosol conditions, it seems likely that above the ocean where aerosol loading is usually low and ASDs often exhibit bimodal shapes with very hygroscopic particles (Wex et al., 2016; Braga et al., 2021), Aitken mode particles are activated to cloud droplets. This confirms findings in marine stratocumulus clouds with moderate $w \geq 0.5$ m s^{-1} (Schulze et al., 2020). Given that marine stratocumuli comprise a large fraction of global cloud coverage, the contribution of Aitken mode particles to N_d above the ocean should thus be included in global estimates of aerosol-cloud interactions. Similarly, our concept is consistent with the large observed fractions of activated Aitken mode particles at Arctic sites (Komppula et al., 2005). Contrary, it implies that in highly polluted regions even high $N_{a,Ait}$ (e.g., in megacities, Mönkkönen et al. (2005)) are not relevant in stratocumulus and shallow cumulus clouds as droplets will only form on accumulation mode particles.

Global model studies have identified large uncertainties in CCN number concentration and N_d predictions due to the assumptions associated with Aitken mode particle properties, specifically in the Southeast US, Europe and to a small extent in the Amazon region (Lee et al., 2013; Chang et al., 2021). Our framework, together with global maps of κ_{Ait} and κ_{acc} (e.g., Chang et al. (2017)), will help reducing these uncertainties and constraining aerosol-cloud interactions in regions where Aitken mode particles affect cloud properties.

Appendix A

Table A1. Definition of parameters that are used in the discussion

Parameter	Description
D_g	Geometric mean mode diameter
$D_{g,Ait}$	Mean Aitken mode diameter
$D_{g,acc}$	Mean Aitken mode diameter
D_{min}	D of smallest particle that forms a cloud droplet
D	Diameter of dry particle
$F_{act,Ait}$	Activated fraction of Aitken mode particles
	$N_{d,Ait}/N_{a,Ait}$
$F_{act,acc}$	Activated fraction of Aitken mode particles
	$N_{d,acc}/N_{a,acc}$
κ	Hygroscopicity parameter
κ_{Ait}	Hygroscopicity parameter for Aitken mode particles
κ_{acc}	Hygroscopicity parameter for
	accumulation mode particles
N_a	Particle number concentration
$N_{a,acc}$	Particle number concentration of
	Aitken mode particles
$N_{a,Ait}$	Particle number concentration of
	accumulation mode particles
N_d	Predicted droplet number concentration
$N_{d,Ait}$	Number concentration of droplets formed on
	Aitken mode particles
$N_{d,acc}$	Number concentration of droplets formed on
	accumulation mode particles
s	Saturation
s_{eq}	Equilibrium saturation based on Köhler theory
S_{max}	supersaturation
σ_g	Geometric standard deviation for mode
w	Updraft velocity
$\xi(\kappa)$	Sensitivity of N_d to κ (Equation E.4)
$\xi(N_a)$	Sensitivity of N_d to N_a (Equation E.5)

Code and data availability. Details on the model codes and further model results can be obtained from the corresponding authors upon request.

Author contributions. MLP and BE led the study and wrote the manuscript with input from all coauthors. MZ and BE performed the model simulations. MZ, RCB, OOK, and UP commented on the manuscript.

Competing interests. The authors declare that they have no conflict of interest.

Acknowledgements. This work has been supported by the French National Research Agency (ANR) (grant no. ANR-17-MPGA- 0013) and the Max Planck Society (MPG).

References

Andreae, M. O. and Rosenfeld, D.: Aerosol-cloud-precipitation interactions. Part 1: The nature and sources of cloud-active aerosols, Earth Science Reviews, 89, 13–41, 2008.

Anttila, T. and Kerminen, V. M.: On the contribution of Aitken mode particles to cloud droplet populations at continental background areas - A parametric sensitivity study, Atmospheric Chemistry and Physics, https://doi.org/10.5194/acp-7-4625-2007, 2007.

Anttila, T., Brus, D., Jaatinen, A., Hyvärinen, A. P., Kivekäs, N., Romakkaniemi, S., Komppula, M., and Lihavainen, H.: Relationships between particles, cloud condensation nuclei and cloud droplet activation during the third Pallas Cloud Experiment, Atmospheric Chemistry and Physics, https://doi.org/10.5194/acp-12-11435-2012, 2012.

Birmili, W., Wiedensohler, A., Heintzenberg, J., and Lehmann, K.: Atmospheric particle number size distribution in central Europe: Statistical relations to air masses and meteorology, Journal of Geophysical Research: Atmospheres, 106, 32 005–32 018, https://doi.org/10.1029/2000JD000220, 2001.

Braga, R. C., Ervens, B., Rosenfeld, D., Andreae, M. O., Förster, J.-D., Fütterer, D., Pardo, L. H., Holanda, B. A., Jurkat, T., Krüger, O. O., Lauer, O., Machado, L. A., Pöhlker, C., Sauer, D., Voigt, C., Walser, A., Wendisch, M., Pöschl, U., and Pöhlker, M. L.: Cloud droplet number closure for tropical convective clouds during the ACRIDICON–CHUVA campaigne, Atmos. Chem . Phys. Discuss., submitted, 2021.

Bulatovic, I., Igel, A. L., Leck, C., Heintzenberg, J., Riipinen, I., and Ekman, A. M. L.: The importance of Aitken mode aerosol particles for cloud sustenance in the summertime high Arctic: A simulation study supported by observational data, Atmospheric Chemistry and Physics Discussions, 2020, 1–28, https://doi.org/10.5194/acp-2020-665, 2020.

Cantrell, W., Shaw, G., and Benner, R.: Cloud properties inferred from bimodal aerosol number distributions, Journal of Geophysical Research Atmospheres, https://doi.org/10.1029/1999JD900252, 1999.

Cecchini, M. A., MacHado, L. A., Andreae, M. O., Martin, S. T., Albrecht, R. I., Artaxo, P., Barbosa, H. M., Borrmann, S., Fütterer, D., Jurkat, T., Mahnke, C., Minikin, A., Molleker, S., Pöhlker, M. L., Pöschl, U., Rosenfeld, D., Voigt, C., Weinzierl, B., and Wendisch, M.: Sensitivities of Amazonian clouds to aerosols and updraft speed, Atmospheric Chemistry and Physics, https://doi.org/10.5194/acp-17-10037-2017, 2017.

Chang, D., Cheng, Y., Reutter, P., Trentmann, J., Burrows, S. M., Spichtinger, P., Nordmann, S., Andreae, M. O., Pöschl, U., and Su, H.: Comprehensive mapping and characteristic regimes of aerosol effects on the formation and evolution of pyro-convective clouds, Atmospheric Chemistry and Physics, 15, 10 325–10 348, https://doi.org/10.5194/acp-15-10325-2015, 2015.

Chang, D. Y., Lelieveld, J., Tost, H., Steil, B., Pozzer, A., and Yoon, J.: Aerosol physicochemical effects on CCN activation simulated with the chemistry-climate model EMAC, Atmospheric Environment, https://doi.org/10.1016/j.atmosenv.2017.03.036, 2017.

Chang, D. Y., Lelieveld, J., Steil, B., Yoon, J., Yum, S. S., and Kim, A.-H.: Variability of aerosol-cloud interactions induced by different cloud droplet nucleation schemes, Atmospheric Research, 250, 105 367, https://doi.org/10.1016/j.atmosres.2020.105367, 2021.

Ervens, B.: Modeling the Processing of Aerosol and Trace Gases in Clouds and Fogs, Chemical Reviews, 115, 4157–4198, https://doi.org/10.1021/cr5005887, 2015.

Ervens, B., Feingold, G., and Kreidenweis, S. M.: Influence of water-soluble organic carbon on cloud drop number concentration, Journal of Geophysical Research D: Atmospheres, https://doi.org/10.1029/2004JD005634, 2005.

Fan, J., Rosenfeld, D., Zhang, Y., Giangrande, S. E., Li, Z., Machado, L. A. T., Martin, S. T., Yang, Y., Wang, J., Artaxo, P., Barbosa, H. M. J., Braga, R. C., Comstock, J. M., Feng, Z., Gao, W., Gomes, H. B., Mei, F., Pöhlker, C., Pöhlker, M. L., Pöschl, U., and

de Souza, R. A. F.: Substantial convection and precipitation enhancements by ultrafine aerosol particles, Science, 359, 411 LP – 418, https://doi.org/10.1126/science.aan8461, 2018.

Fanourgakis, G. S., Kanakidou, M., Nenes, A., Bauer, S. E., Bergman, T., Carslaw, K. S., Grini, A., Hamilton, D. S., Johnson, J. S., Karydis, V. A., Kirkeväg, A., Kodros, J. K., Lohmann, U., Luo, G., Makkonen, R., Matsui, H., Neubauer, D., Pierce, J. R., Schmale, J., Stier, P., Tsigaridis, K., Van Noije, T., Wang, H., Watson-Parris, D., Westervelt, D. M., Yang, Y., Yoshioka, M., Daskalakis, N., Decesari, S., Gysel-Beer, M., Kalivitis, N., Liu, X., Mahowald, N. M., Myriokefalitakis, S., Schrödner, R., Sfakianaki, M., Tsimpidi, A. P., Wu, M., and Yu, F.: Evaluation of global simulations of aerosol particle and cloud condensation nuclei number, with implications for cloud droplet formation, Atmospheric Chemistry and Physics, https://doi.org/10.5194/acp-19-8591-2019, 2019.

Feingold, G.: Modeling of the first indirect effect: Analysis of measurement requirements, Geophysical Research Letters, https://doi.org/10.1029/2003GL017967, 2003.

Feingold, G. and Heymsfield, A. J.: Parameterizations of condensational growth of droplets for use in general circulation models, Journal of the Atmospheric Sciences, https://doi.org/10.1175/1520-0469(1992)049<2325:POCGOD>2.0.CO;2, 1992.

Feingold, G. and Kreidenweis, S.: Does cloud processing of aerosol enhance droplet concentrations?, J. Geophys. Res., 105, 24 351–24 361, https://doi.org/10.1029/2000JD900369, 2000.

Gérémy, G., Wobrock, W., Flossmann, A. I., Schwarzenböck, A., and Mertes, S.: A modelling study on the activation of small Aitken-mode aerosol particles during CIME 97, Tellus B: Chemical and Physical Meteorology, 52, 959–979, https://doi.org/10.3402/tellusb.v52i3.17078, 2000.

Gunthe, S. S., King, S. M., Rose, D., Chen, Q., Roldin, P., Farmer, D. K., Jimenez, J. L., Artaxo, P., Andreae, M. O., Martin, S. T., and Pöschl, U.: Cloud condensation nuclei in pristine tropical rainforest air of Amazonia: Size-resolved measurements and modeling of atmospheric aerosol composition and CCN activity, Atmospheric Chemistry and Physics, https://doi.org/10.5194/acp-9-7551-2009, 2009.

Hammer, E., Bukowiecki, N., Luo, B. P., Lohmann, U., Marcolli, C., Weingartner, E., Baltensperger, U., and Hoyle, C. R.: Sensitivity estimations for cloud droplet formation in the vicinity of the high-alpine research station Jungfraujoch (3580 m a.s.l.), Atmospheric Chemistry and Physics, https://doi.org/10.5194/acp-15-10309-2015, 2015.

Heintzenberg, J., Birmili, W., Wiedensohler, A., Nowak, A., and Tuch, T.: Structure, variability and persistence of the submicrometre marine aerosol, Tellus B: Chemical and Physical Meteorology, 56, 357–367, https://doi.org/10.3402/tellusb.v56i4.16450, 2004.

Hoppel, W. A., Frick, G. M., and Larson, R. E.: Effect of nonprecipitating clouds on the aerosol size distribution in the marine boundary layer, Geophysical Research Letters, 13, 125–128, https://doi.org/10.1029/GL013i002p00125, 1986.

Jung, C. H., Yoon, Y. J., Kang, H. J., Gim, Y., Lee, B. Y., Ström, J., Krejci, R., and Tunved, P.: The seasonal characteristics of cloud condensation nuclei (CCN) in the arctic lower troposphere, Tellus B: Chemical and Physical Meteorology, 70, 1–13, https://doi.org/10.1080/16000889.2018.1513291, 2018.

Köhler, H.: The nucleus in and the growth of hygroscopic droplets, Transact. Faraday Soc., 32, 1152–1161, 1936.

Komppula, M., Lihavainen, H., Kerminen, V. M., Kulmala, M., and Viisanen, Y.: Measurements of cloud droplet activation of aerosol particles at a clean subarctic background site, Journal of Geophysical Research D: Atmospheres, https://doi.org/10.1029/2004JD005200, 2005.

Korhonen, H., Carslaw, K. S., Spracklen, D. V., Ridley, D. A., and Ström, J.: A global model study of processes controlling aerosol size distributions in the Arctic spring and summer, Journal of Geophysical Research: Atmospheres, 113, https://doi.org/10.1029/2007JD009114, 2008.

Kulmala, M., Korhonen, P., Vesala, T., Hansson, H.-C., Noone, K., and Svenningsson, B.: The effect of hygroscopicity on cloud droplet formation, Tellus B: Chemical and Physical Meteorology, 48, 347–360, https://doi.org/10.3402/tellusb.v48i3.15903, 1996.

Lee, L. A., Pringle, K. J., Reddington, C. L., Mann, G. W., Stier, P., Spracklen, D. V., Pierce, J. R., and Carslaw, K. S.: The magnitude and causes of uncertainty in global model simulations of cloud condensation nuclei, Atmospheric Chemistry and Physics, https://doi.org/10.5194/acp-13-8879-2013, 2013.

Loftus, A. M.: Towards an enhanced droplet activation scheme for multi-moment bulk microphysics schemes, Atmospheric Research, 214, 442–449, https://doi.org/10.1016/j.atmosres.2018.08.025, 2018.

McFiggans, G., Artaxo, P., Baltensperger, U., Coe, H., Facchini, M. C., Feingold, G., Fuzzi, S., Gysel, M., Laaksonen, A., Lohmann, U., Mentel, T. F., Murphy, D. M., O'Dowd, C. D., Snider, J. R., and Weingartner, E.: The effect of physical and chemical aerosol properties on warm cloud droplet activation, Atmospheric Chemistry and Physics, https://doi.org/10.5194/acp-6-2593-2006, 2006.

Mönkkönen, P., Koponen, I. K., Lehtinen, K. E., Hämeri, K., Uma, R., and Kulmala, M.: Measurements in a highly polluted Asian mega city: Observations of aerosol number size distribution, modal parameters and nucleation events, Atmospheric Chemistry and Physics, https://doi.org/10.5194/acp-5-57-2005, 2005.

Moore, R. H., Karydis, V. A., Capps, S. L., Lathem, T. L., and Nenes, A.: Droplet number uncertainties associated with CCN: An assessment using observations and a global model adjoint, Atmospheric Chemistry and Physics, https://doi.org/10.5194/acp-13-4235-2013, 2013.

Pardo, L. H., MacHado, L. A. T., Cecchini, M. A., and Gácita, M. S.: Quantifying the aerosol effect on droplet size distribution at cloud top, Atmospheric Chemistry and Physics, https://doi.org/10.5194/acp-19-7839-2019, 2019.

Petters, M. D. and Kreidenweis, S. M.: A single parameter representation of hygroscopic growth and cloud condensation nucleus activity, Atmospheric Chemistry and Physics, https://doi.org/10.5194/acp-7-1961-2007, 2007.

Pöhlker, M. L., Pöhlker, C., Ditas, F., Klimach, T., De Angelis, I. H., Araújo, A., Brito, J., Carbone, S., Cheng, Y., Chi, X., Ditz, R., Gunthe, S. S., Kesselmeier, J., Könemann, T., Lavrič, J. V., Martin, S. T., Mikhailov, E., Moran-Zuloaga, D., Rose, D., Saturno, J., Su, H., Thalman, R., Walter, D., Wang, J., Wolff, S., Barbosa, H. M., Artaxo, P., Andreae, M. O., and Pöschl, U.: Long-term observations of cloud condensation nuclei in the Amazon rain forest - Part 1: Aerosol size distribution, hygroscopicity, and new model parametrizations for CCN prediction, Atmospheric Chemistry and Physics, https://doi.org/10.5194/acp-16-15709-2016, 2016.

Pöhlker, M. L., Ditas, F., Saturno, J., Klimach, T., Hrabě De Angelis, I., Araùjo, A. C., Brito, J., Carbone, S., Cheng, Y., Chi, X., Ditz, R., Gunthe, S. S., Holanda, B. A., Kandler, K., Kesselmeier, J., Könemann, T., Krüger, O. O., Lavric, J. V., Martin, S. T., Mikhailov, E., Moran-Zuloaga, D., Rizzo, L. V., Rose, D., Su, H., Thalman, R., Walter, D., Wang, J., Wolff, S., Barbosa, H. M., Artaxo, P., Andreae, M. O., Pöschl, U., and Pöhlker, C.: Long-term observations of cloud condensation nuclei over the Amazon rain forest - Part 2: Variability and characteristics of biomass burning, long-range transport, and pristine rain forest aerosols, Atmospheric Chemistry and Physics, https://doi.org/10.5194/acp-18-10289-2018, 2018.

Polonik, P., Knote, C., Zinner, T., Ewald, F., Kölling, T., Mayer, B., Andreae, M. O., Jurkat-Witschas, T., Klimach, T., Mahnke, C., Molleker, S., Pöhlker, C., Pöhlker, M. L., Pöschl, U., Rosenfeld, D., Voigt, C., Weigel, R., and Wendisch, M.: The challenge of simulating the sensitivity of the Amazonian cloud microstructure to cloud condensation nuclei number concentrations, Atmos. Chem. Phys., 20, 1591–1605, https://doi.org/10.5194/acp-20-1591-2020, 2020.

Pruppacher, H. R. and Klett, J. D.: Microphysics of clouds and precipitation, Kluwer Academics Publisher, Dordrecht (NL), 2<sup>nd</edn., 2003.

Pöhlker, M. L., Krüger, O. O., Förster, J.-D., Elbert, W., Fröhlich-Nowoisky, J., Pöschl, U., Pöhlker, C., Bagheri, G., Bodenschatz, E., Huffman, J. A., Scheithauer, S., and Mikhailov, E.: Respiratory aerosols and droplets in the transmission of infectious diseases, arXiv, https://doi.org/arXiv:2103.01188, 2021.

Reutter, P., Su, H., Trentmann, J., Simmel, M., Rose, D., Gunthe, S. S., Wernli, H., Andreae, M. O., and Pöschl, U.: Aerosol- and updraft-limited regimes of cloud droplet formation: influence of particle number, size and hygroscopicity on the activation of cloud condensation nuclei (CCN), Atmos. Chem. Phys., 9, 7067–7080, https://doi.org/10.5194/acp-9-7067-2009, 2009.

Reutter, P., Trentmann, J., Seifert, A., Neis, P., Su, H., Chang, D., Herzog, M., Wernli, H., Andreae, M. O., and Pöschl, U.: 3-D model simulations of dynamical and microphysical interactions in pyroconvective clouds under idealized conditions, Atmospheric Chemistry and Physics, 14, 7573–7583, https://doi.org/10.5194/acp-14-7573-2014, 2014.

Roelofs, G. J., Stier, P., Feichter, J., Vignati, E., and Wilson, J.: Aerosol activation and cloud processing in the global aerosol-climate model ECHAM5-HAM, Atmospheric Chemistry and Physics, https://doi.org/10.5194/acp-6-2389-2006, 2006.

Rose, D., Gunthe, S. S., Mikhailov, E., Frank, G. P., Dusek, U., Andreae, M. O., and Pöschl, U.: Calibration and measurement uncertainties of a continuous-flow cloud condensation nuclei counter (DMT-CCNC): CCN activation of ammonium sulfate and sodium chloride aerosol particles in theory and experiment, Atmospheric Chemistry and Physics, 8, 1153–1179, https://doi.org/10.5194/acp-8-1153-2008, 2008.

Schulze, B. C., Charan, S. M., Kenseth, C. M., Kong, W., Bates, K. H., Williams, W., Metcalf, A. R., Jonsson, H. H., Woods, R., Sorooshian, A., Flagan, R. C., and Seinfeld, J. H.: Characterization of Aerosol Hygroscopicity Over the Northeast Pacific Ocean: Impacts on Prediction of CCN and Stratocumulus Cloud Droplet Number Concentrations, Earth and Space Science, https://doi.org/10.1029/2020EA001098, 2020.

Ward, D. S., Eidhammer, T., Cotton, W. R., and Kreidenweis, S. M.: The role of the particle size distribution in assessing aerosol composition effects on simulated droplet activation, Atmos. Chem. Phys., 10, 5435–5447, https://doi.org/10.5194/acp-10-5435-2010, 2010.

Wex, H., Dieckmann, K., Roberts, G. C., Conrath, T., Izaguirre, M. A., Hartmann, S., Herenz, P., Schäfer, M., Ditas, F., Schmeissner, T., Henning, S., Wehner, B., Siebert, H., and Stratmann, F.: Aerosol arriving on the Caribbean island of Barbados: Physical properties and origin, Atmospheric Chemistry and Physics, 16, 14 107–14 130, https://doi.org/10.5194/acp-16-14107-2016, 2016.

Zhou, J., Swietlicki, E., Hansson, H. C., and Artaxo, P.: Submicrometer aerosol particle size distribution and hygroscopic growth measured in the Amazon rain forest during the wet season, Journal of Geophysical Research: Atmospheres, 107, LBA 22–1–LBA 22–10, https://doi.org/10.1029/2000JD000203, 2002.